5-2007

Energy Harvesting using Optimized Piezoelectric Microcantilevers

Ahmed Mohamed Elalfy
University of Tennessee - Knoxville

To the Graduate Council:

I am submitting herewith a thesis written by Ahmed Mohamed Elalfy entitled "Energy Harvesting using Optimized Piezoelectric Microcantilevers." I have examined the final electronic copy of this thesis for form and content and recommend that it be accepted in partial fulfillment of the requirements for the degree of Master of Science, with a major in Mechanical Engineering.

Arnold Lumsdaine, Major Professor

We have read this thesis and recommend its acceptance:

S. Islam, J. Landes

Accepted for the Council:
Carolyn R. Hodges

Vice Provost and Dean of the Graduate School

(Original signatures are on file with official student records.)

Graduate Council:

I am submitting herewith a thesis written by Ahmed Mohamed Elalfy entitled "Energy Harvesting using Optimized Piezoelectric Microcantilevers". I have examined the final electronic copy of this thesis for form and content and recommend that it be accepted in partial fulfillment of the requirements for the degree of Master of Science, with a major in Mechanical Engineering.

Arnold Lumsdaine

_____

Major Professor

We have read this thesis
and recommend its acceptance:

S. Islam

_____

J. Landes

_____

Accepted for the Council:

Linda Painter

_____

Interim Dean of
the Graduate School

(Original signatures are on file with official student records.)

Energy Harvesting Using Optimized Piezoelectric Micro-cantilevers

A Thesis
Presented for the
Master of Science
Degree
The University of Tennessee, Knoxville

Ahmed Mohamed Elalfy
May 2007.

Acknowledgments

An unending amount of appreciation and gratitude goes to Dr. Lumsdaine whose initiative, support, encouragement, and dedication made this thesis possible. Having a mentor and advisor with such integrity definitely makes me feel more confident about the knowledge I have received and the person I have become over the past few years especially.

I thank Dr. Islam for his light heartedness and ease of communication; I always feel welcomed to approach and converse with him and have a great sense of inspiration afterwards, thank you.

A great deal of thanks also goes out to Dr. Landes who has been an excellent professor and was able to make such a sacrifice at last minute to be able to help me; I appreciate your kindness.

Thank you to Dr. Thundat who was very keen on being part of this work and who showed a lot of enthusiasm, I appreciate your effort.

Thank you very much to Mohan Damu and Mathew Parsons who I feel are part authors in this work for their invaluable input and continued support; you guys have been nothing shy of great friends and great colleagues.

Thank you to Harish Valluru for being very accommodating, for your ideas, and always having a smile.

Thank you Shing-Jia Tang for giving me encouragement and setting a goal for me to be in the lab before he does, which I was able to accomplish once or twice.

In addition I would like to thank my close friends Nghi Dinh and James Crawford among many others, who were always there for support and encouragement when I needed it, thanks guys.

Of course an endless amount of gratitude to my loving family in Florida, Georgia, and Michigan, who always trusted in me and helped strengthen my faith in God. They made me believe dreams can come true.

Abstract

In this thesis, the energy producing capabilities and efficiency of Piezoelectric materials for ambient energy harvesting from multi-layered micro-cantilevers are analyzed. The cantilevers are then optimized utilizing a homogenization approach involving the redistribution of materials in all regions throughout the three dimensional model to yield the greatest voltage output for a specified tip force under static loading; This would be analogous to having the greatest energy production. The design of the model using the Finite Element Analysis (FEA) software ABAQUS is used in conjunction with a commercial FORTRAN optimization code, where the FEA software handles the mechanical design aspect of creating the model and determining nodal voltage quantities and the FORTRAN code executes the optimization procedure for maximizing the Voltage production. The optimization uses a Sequential Quadratic Programming (SQP) algorithm. An optimal case is found and its topology follows the expected tapered shape.

TABLE OF CONTENTS

LIST OF TABLES

LIST OF FIGURES

NOMENCLATURE

σ	Mechanical Stress
S	Mechanical Strain
Y	Elastic Modulus
E	Electric Field
G	Shear Modulus
ω_n	Natural Frequency
X	X_i is the i'th design variable.
PZT	Lead Zirconate Titanate
PVDF	Polyvinylidene Fluoride
MEMS	Microelectromechanical systems
g	Piezoelectric Stress Constant
D	Charge Density Distribution
d	Piezoelectric Strain Constant
ε	Piezoelectric Electric Permittivity
ε_r	Relative Permittivity
ε_o	Permittivity of Free Space
A	Layer Surface Area
A_{XS}	Cross Sectional Area
Q	Charge

C	Capacitance
V	Voltage/Electric Potential
t	Thickness
q	Lateral Loading on Beam
M	Bending Moment
I	Moment of Inertia
κ	Curvature
λ	Linear Mass Density
ρ	Volumetric Mass Density

CHAPTER 1: INTRODUCTION

1.1 MOTIVATION

The conversion of the ambient energy surrounding a system into usable electrical energy is known as energy harvesting. A motivation for energy harvesting has stemmed from technological advances in low-power micro-electromechanical systems (MEMS). The potential use of embedded wireless sensors that are self-powered has attracted interest as the implications would promise safety improvements and cost reductions in monitoring the health of structures. The remote sensing enables data to be collected from otherwise inaccessible locations. This has application in the Aerospace, Biomedical, and Civil industries, where sensors can be used without battery limitations.

Because of their small size and relatively simple fabrication (which can easily be scaled for developing a large array), microcantilever arrays are a candidate for energy harvesting. The typical microcantilever configuration consists of a substrate layer, which can have a thinner piezoelectric layer on one or both sides. With the layers bonded together, an electric potential difference is produced in the piezoelectric layer from ambient vibrations. This may be harnessed through a DC voltage rectifier, a capacitor, or a battery incorporated into an electrical harvesting circuit to supply the power required for wireless radio communication.

Some of the approaches taken in the past for powering wireless devices include scavenging solar, thermal, and ambient environmental vibration energy. Ambient vibrations can be a potential source for generating power at levels equivalent to lithium batteries (Sodano et. al., 2002), (Sodano et. al., 2004). In this study, the voltage levels that can be achieved by energy harvesting microcantilevers are examined. A finite element bi-layer beam is created in both 2D and 3D forms to compare and validate. A commercially available Finite Element Analysis (FEA) code, ABAQUS, is used for the finite element modeling. The elements used in the 2D model are 8 noded quadratic elements and the 3D model utilizes 8 noded linear elements for both the piezoelectric and aluminum elements. The microcantilever is made up of a piezoelectric layer supported by a substrate layer, which is aluminum. The natural frequencies are determined and an element convergence study is performed. Another area of study is the topology optimization of the microcantilevers. This leads to a more efficient design where the cantilevers are optimally configured in such a way that as much of the vibrations realized from the energy source can be utilized as storable energy. Topology optimization is performed on the microcantilevers using a homogenization approach to maximize voltage production in the piezoelectric layer. NLPQL, a Sequential Quadratic Programming (SQP) based program, handles the optimization and a FORTRAN code was developed to link the FEA software with the optimization to yield the desired results. In addition, various

piezoelectric materials are considered as a parameter study to determine their suitability for energy reclamation.

1.2 INTRODUCTION

The past several years have seen a rapid increase in the development of Microelectromechanical Systems (MEMS). There is a compelling desire for devices to be compact, self-powered and portable. This can be attained by absorbing the energy surrounding a system and converting it into a form of usable electrical energy. This is defined as Energy Harvesting. Several methods of energy harvesting have been developed. This has contributed much to the development of MEMS devices which operate with low power. MEMS devices such as wireless sensors are devices that measure physical quantities (Thundat,1997). This is achieved by using the variation in the physical properties of these microstructures. Advancements in the fabrication processes of these micro-systems have further aided their development. Such devices could potentially be used for a wide variety of applications. A few possible applications include: monitoring structural integrity in buildings, strain measurements in implants, data measurements in hostile environments such as in space or on the tips of aircraft wings, determining the location of persons in commercial buildings to control the environment in a more energy efficient manner, sensing harmful chemical agents in high traffic areas, monitoring fatigue crack formation on aircraft, monitoring pressure in automobile tires, global positioning system (GPS)

tracking devices on animals in the wild, etc. It is becoming a general consensus that very low power embedded electronic devices will become a ubiquitous part of our environment, performing functions in applications ranging from entertainment to factory automation (Umeda et. al. 1997).

Developments in low power integrated circuit production and design have reduced the power consumption of a wireless sensor to less than 1mW. The problem of powering current sensors comes to light when the issue of replacing batteries is addressed. In order to replace the batteries, the sensor must be retrieved and the battery replaced. Because of the remote locations of these wireless sensors, getting to the sensors simply to replace the battery can be an expensive and tedious if not impossible task. For example, in a weight bearing civil infrastructure that has an embedded wireless sensor, replacing the battery can be unfeasible. State of the art, non-rechargeable lithium batteries can provide up to 800 WH/L (Watt hours per liter) or 2880 J/cm^3. If an electronic device with a 1 cm^3 battery were to consume 100 μW of power on average (an aggressive goal), the device could last 8000 hours or 333 days, almost a year. It is worth mentioning that the sensors and electronics of a wireless sensor node will be far smaller than 1 cm^3, so, in this case, the battery would dominate the system volume. Clearly, a lifetime of 1 year is far from sufficient (duToit, 2005).

Vibrations are prevalent in many systems with sensor applications and are a good source of energy. The application of piezoelectric materials which can easily

utilize these vibrations is one method that has potential for use in energy harvesting. The crystalline structure of Piezoelectric materials enables them to couple the mechanical and electrical domains with very little loss. A mechanical strain applied to the material produces an electrical potential and vice versa. This ability of these materials can be capitalized by transforming mechanical energy surrounding a system, commonly ambient vibration, and transforming it into electrical energy which can be stored in a battery or capacitor.

The aim of this work is to design a vibration based piezoelectric generator that can efficiently realize a harmonic tip force input and convert it to an electrical potential. Cantilever bi-layer models consisting of a top layer of piezoelectric material and a substrate layer of an elastic material such as Aluminum are studied. Topology Optimization is performed on both layers of the cantilever to maximize electric potential output. The Finite Element Analysis software ABAQUS has the capability of modeling piezoelectric materials and is used to design the micro-cantilever. Both 2-D and 3-D models are developed where 8-noded quadratic elements are used. The optimization is performed with a gradient based optimization code which uses a sequential quadratic programming algorithm. Gradients are calculated numerically using the finite difference method. Results show a significant increase in electrical potential produced which can be translated to increased power production.

1.3 BRIEF PROBLEM STATEMENT AND GOALS

The design of the micro-scale piezoelectric microcantilever is the first step. An equally thick layer of a piezoelectric material and an aluminum substrate are the constituents of the structure. Once the model is setup and the appropriate boundary conditions are applied, the natural frequencies are determined. The tip deflection induced by a tip force is also studied which leads to an inquiry into the stress and strain distribution along the cantilever beam. From the strain induced in the piezoelectric section of the beam, the voltage can be determined. This can all be achieved in ABAQUS. Since the power or energy production is related to the voltage, the FORTRAN code can then be utilized to distribute material to or away from the areas of greatest or least strain in both the piezoelectric and aluminum substrate layers in order to maximize the voltage production. This is the topology optimization aspect of the study.

CHAPTER 2: BACKGROUND STUDIES

2.1 BACKGROUND RESEARCH

Piezoelectric materials have a crystalline structure that permits them to be used as mechanisms capable of transforming mechanical energy, commonly found as ambient vibration, into electrical energy that can be used to power devices. Portable electronics can be developed by applying power harvesting devices that do not depend on finite energy sources, namely batteries. This yields major advances on the applications possible with these systems. Wireless sensors can now be placed in remote or hostile locations, such as in weight bearing members in civil infrastructure (Sirohi et. al. 2000) or within close proximity to the core of a nuclear reactor respectively.

The crystalline structure of the piezoelectric material that enables it to couple the mechanical and electrical domains has a measuring factor known as coupling coefficient. This relates the strain to the material to the electrical potential produced. As vibrations are the source of energy, the objective is to maximize the voltage output of the piezoelectric material. Since cantilever beams have been extensively studied and analytical solutions have been developed, a common approach of maximizing the strain from vibrations is with the use of a layered cantilever beam. A common design is a bi-layer cantilever where the top layer is piezoelectric and the bottom, or substrate layer is an elastic material such as aluminum. This design enables a tip force to be applied to one end of the cantilever design. With the beam constrained at the opposite end, this tip

force creates the greatest strain in the piezoelectric layer in the region closest to the constraint or boundary condition of the beam. By optimizing the allocation of material to regions of greatest strain while reducing the amount of material in regions of increased stiffness, greater voltages can be realized for the same forces acting on the cantilever. The optimization approach utilizes the idea of homogenization, where the material fractions of individual elements are allowed to change which in turn varies the material properties of the elements. In the case of the Aluminum (substrate) layer, the elastic modulus and density are directly proportional to the material fractions. In the piezoelectric layer, in addition to the stiffness and density varying proportionately with material fractions, the dielectric constants vary with material fractions, however, this was in a non-linear manner.

2.1.1 PIEZOELECTRIC MATERIAL HISTORY

Piezin, the Greek word 'to press', describes Piezoelectricity as 'pressure electricity'. Piezoelectricity was discovered in the 1880's by the Currie brothers when they found that when introduced to an electrical field, Quartz deformed. In 1916, the French physicist Paul Langevin, who was known for his ultrasonic work in the development of SONAR using a quartz transmitter and receiver, created one of the first practical applications of the Piezoelectric effect. Not long after Piezoceramics were developed, the phonograph pickup produced using Barium

Titanate ($BATiO_3$) was designed in 1947. 1955 was the year in which the most widely used piezoceramic Lead Zirconate Titanate (PZT) was developed. Following the discovery of small piezoelectric effects in the bones of whales in the 1960's, researchers began an intensive study into organic materials and ferroelectric polymers. Studies were started by pioneers such as Fukada et. al,1979). who discovered induced charges on the surface of rolled films of polypeptides. In 1969, a major discovery was made when Kawai discovered a strong piezoelectric effect in Polyvinyldene Flouride (PVDF), which led to another important discovery in 1975 of PVDF's strong pyroelectric effect.

Piezoelectric materials can be sub-categorized into 3 types:-

Ceramics:	Including Barium Titanate (BATiO3), Lead Zirconium Titanate (PZT), Lead Metaniobate (PLZT), and Lead Magnesium Niobate (PMN)
Crystalline Structures:	Quartz and Rochelle salt
Polymers:	Polyvinyldene Flouride (PVDF), Polypeptide, PVC, and Nylon.

Piezo-electric transducers are a multi-billion dollar industry with piezoelectric polymer sensors being one of the fastest growing due to its vastly wide integration into microprocessor applications. Recent advances in low power consumption circuits have driven the exploration into embedded wireless sensors.

2.1.2 PIEZOELECTRICS: A CONCEPTUAL OVERVIEW

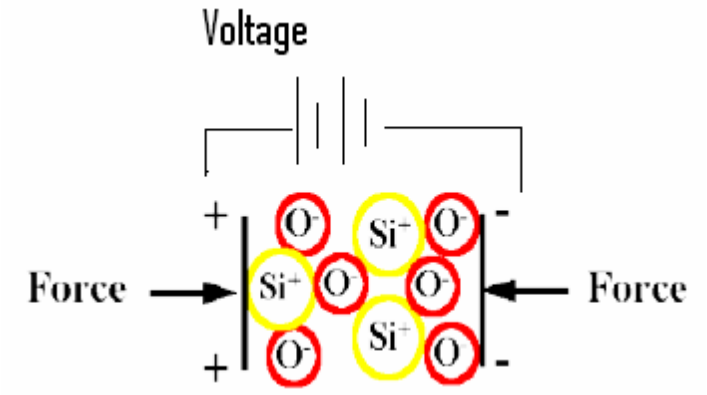

Figure 2.1: The Piezoelectric effect (Jaffe et. al. 1954)

Figure 2.1 illustrates the piezoelectric effect. The essence of piezoelectricity is the coupling between the mechanical and electrical attributes of a material, where electrical energy can be converted into mechanical energy and vice versa. A temporary re-alignment of molecules occurs when a force is applied to a piezoelectric material; this induced strain causes a temporary dipole in the unit cell.

The coupling of the mechanical and electrical domains depends on the dimensions and geometries of the piezoelectric material, the coupling coefficient and dielectric properties, and the direction in which the mechanical or electrical excitation is applied. This effect occurs naturally in quartz crystals, but can be induced in other materials, such as specially formulated ceramics consisting mainly of Lead, Zirconate, and Titanate (PZT). Because they are ceramics (piezoceramics), they can be formed to most any shape or size. In order to activate/initiate the piezoelectric properties, the material is first heated to its

Curie temperature. A voltage field of sufficient magnitude is applied at this state in the desired direction, forcing the ions to realign along this polling axis. The ions retain this formation as the ceramics cools and act accordingly.

The constitutive equations define the interaction between a piezoelectric material's electric field, E, charge density distribution, D, and mechanical stress and strain, σ and S respectively.

If the matrix d contains the piezoelectric strain coefficients, piezoelectric constitutive relationships are:

$$S = s_E \sigma + d' E$$
$$D = d\sigma + \varepsilon_\sigma E$$

A more basic relationship can be described when isolating force or poling vectors to a single mode. There is a parameter for the strain constant and the stress constant. The piezoelectric stress constant, g_{ij}, relates the open circuit electric field to a mechanical stress applied. The voltage through the material can be determined easily when the applied electric field and thickness it is applied through is known. The stress constant is then defined as:

$$g_{ij} = \frac{E}{\sigma} = \frac{V/M}{N/M^2}$$

under electrically fixed conditions, or when charge is equal to zero. Another important parameter is the electro-mechanical coupling coefficient, k_{ij}, which is a

measure of how well the material converts electrical energy to mechanical energy and vice versa:-

$$k_{ij} = \sqrt{\frac{We}{Wm}} = \%$$

Beam applications generally use the 31-mode of piezoelectric operation. Depending on the dielectric poling direction, an applied field through the thickness, 3-direction, induces a strain in the 1-direction, along the length. Figures 2.2 and 2.3 illustrate the details of the orientations.

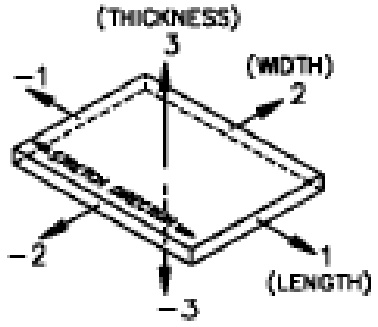

Figure 2.2: Illustration of Co-ordinate Definition (Ikeda, 1990)

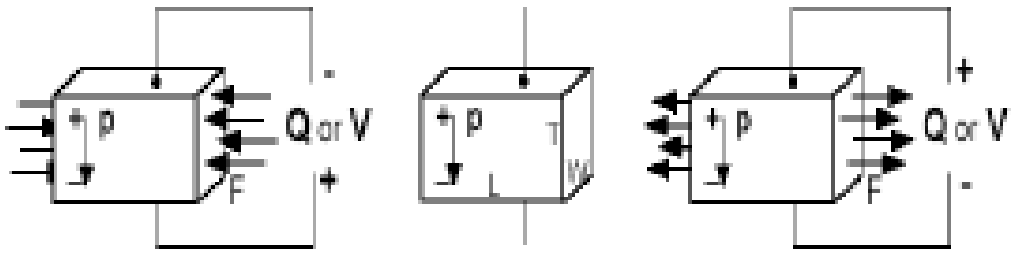

Figure 2.3: Illustration of Voltage Direction with respect to Force (Ikeda, 1990)

Much reference is made to piezoelectric axes and their relation to the poling axis. Convention and the IEEE standard on piezoelectricity state that the poling axis be termed the "3" direction with the same positive/negative sense as the applied voltage field. The remainder of the coordinate system is analogous to a right handed orthogonal system, mapping x-1, y-2, and z-3.

2.1.3 COMPARISON OF COMMON PIEZOELECTRIC MATERIALS

Three of the most common piezoelectric materials are compared in the following table to identify the strong and weak points inherent in each.

With energy harvesting being the primary objective, the better electro-mechanical coupling coefficient, k_{31}, is desired. The PZT is can convert about 2.5 times more mechanical energy into electrical energy than PVDF film and about 33% better than Barium Titanate. In addition, the PZT can convert approximately 5 times more force into charge than PVDF as illustrated by the dielectric constant d_{31}. On the other hand, PVDF is almost 22 times more responsive to an applied force with respect to voltage generation than PZT, as the piezoelectric stress constant, g_{31}, shows.

PZT demonstrates that it is the more capacitive source as capacitance is proportional to the permittivity. The properties of these materials is presented in table 2.1.

Table 2.1: Piezoelectric Material Comparison (www.Piezo.com, www.texloc.com)

Material Property	Units	PSI-5H4E (**PZT**)	BaTiO3	PVDF Film
Density	10^3 kg/m^3	7.5	5.7	1.78
Relative Permittivity	φ/φ_0	1200	1700	12
D_{31} Constant	10^{-12} C/N	110	78	23
G_{31} Constant	10^{-3} Vm/N	10	5	216
K_{31} Constant	% at 1 KHz	30	21	12
Acoustic Impedance	10^6 Kg/m^2-sec	30	30	2.7
Elastic Modulus	GPa	62	67	1.1

The superior electromechanical coupling coefficient of PZT makes it the most desirable material from the ones listed.

In addition, the synthesis and polymerization of PVDF is a complicated process.

2.2 LITERATURE SURVEY

2.2.1 POWER GENERATION

Harvesting power from breathing has been examined by Hausler (1984) where piezoceramic patches were implanted into a dog that utilized the expansion of the rib cage during inspiration part of breathing. They estimate that it takes between 0.1W and 40W to power pulmonary ventilation. Therefore, in order to extract 1mW under the assumption of 20% coupling coefficient, 5mW would be needed, which is very small in comparison. PVDF was used that had 15 %

coupling coefficient. A Voltage of 18V was realized and 17 μW of constant power was produced. Even though this power level seemed small, it is promising that such a simple design had the capacity to operate as demonstrated.

Body heat, blood/breath pressure, movements of the limbs, and chest expansion all have the potential in the interest of energy harvesting. Starner (1996) discusses the feasibilities of these sources and comes to the conclusion that walking has the greatest potential for energy conversion. Up to 5W can be generated from a 52 Kg person taking 2 strides per second using PVDF sole inserts. His study discusses how low power computers that could be worn and used only use 0.5 W.

A similar shoe insert using "Thunder" actuators is developed by Kendall (1998) and uses a PZT unimorph that is oriented on a curved steel base and is prestressed. Both PZT and PVDF are compared where PZT is placed at the heel of the shoe and PVDF is placed under the ball of the foot. This gives the most bending strain, which yields the greatest electrical potential. Because of its curved shape this is more difficult attach to the shoe. PZT produced a peak voltage of 50 V corresponding to a 15 mW power level at 2 Hz whereas the PVDF made a peak voltage of 15 V and 2 mW. Overall, the generator produced an RMS voltage of 1.8 V and 250 mW across a 100 Ω resistor and PVDF is selected for being more inert than PZT.

An energy harvesting eel has been developed by Allen (2001) that consists of a piezoelectric membrane that moves in the wake of a traveling body in fluid.

Oscillations are transmitted to the membrane and consequentially, a charge is produced due to the vortex shredding downstream. This charge can be used to charge a battery powering a device in a remote region. This of course depends on a continuous flow of the fluid, such as an oceanic current or a high atmospheric wind flow.

A 400 μW power generator was developed by Amirtharajah (1998) based on a moving magnetic electromagnetic transducer. Environmental vibrations were shown to power an ultra-low power controller chip which uses delay feedback to control voltages. The model used had a mass of 0.5 g, a spring constant of 174 N/m, and a resulting natural frequency of 94 Hz.

2.2.2 MODELLING OF PIEZOELECTRIC PLATES AND BEAMS

Exact 3D solutions for a laminated piezoelectric model have been developed by Heyliger (1997) where Raleigh-Ritz method solutions are applied for free-vibrations in simply supported piezoelectric plates. Single layer and general theories are used to determine deflection and electric potential on various cases of laminated thick and thin plates. For the thick plates, only the generalized coupled theories prove adequate, and the plates are piecewise non-linear. Normal stress was shown to be predicted by the generalized theories within the piezoelectric thin layer plates as long as the number of layers did not exceed 25. Delamination of the piezoelectric layers is caused by shear stress and is harder to

predict. A better estimate calculation was suggested using pointwise integration of the stress equilibrium equations.

Wang et. al. (2004) discuss a novel approach to detecting and measuring physical, chemical, and biological signals. Full integration, low cost, ease of use, and the capability of manipulating large arrays are motivations that drive the study. A design method is presented for laminated piezoresistive micro-cantilevers to obtain optimal performance. Optimization is applied to the dimensions of the microcantilevers and doping concentrations of the piezoresistors. The thickness and doping concentrations were optimized using static analyses and power densities of noise to generate the best sensitivity and resolution. Finite element models were developed for verification. A method based on non-linear programming is given to facilitate the solving process and the author claims that these methods and conclusions are also applicable to develop other types of piezoresistive laminated sensors and structures.

2.2.3 OPTIMIZATION AND HOMOGENIZATION

Kikuchi and Bensoe (1988) first proposed the idea of topology optimization through homogenization, which is an automated process of finding an optimal structural design. For a given set of boundary conditions and design specifications (constraints), a topology can be computed that is optimal in terms of a mathematical cost function. The authors described the optimal structure as the optimal distribution of material.

Studies have been done (Beuhler, 2004) on how to optimize the topology of piezoelectric materials. Beuhler's work discusses how to attain the different densities and associated properties of constituent material in the defined regions of the design domain by parametrically defining a microstructure that has a variable size hole. The optimal topology is solved for by discretizing the design domain into a finite element grid, each element having been defined parametrically, and therefore possibly varying in density between 0 - 100%. This permits simultaneous design of the structure where material definitions can be assigned in a manner that the objective function is optimized whilst satisfying the constraints and bounds on the parameters. A similar optimization approach was integrated in the shape optimization of unconstrained viscoelestic layers using continuum elements by Lumsdaine et. al. (1998).

CHAPTER 3: Modeling

3.1 FINITE ELEMENT MODEL

A 2D model was initially created as an introductory step to the finite element process as shown in figure 3.1.

Five Piezoelectric and five aluminum elements were created as shown, where elements 1 through 5 were assigned with aluminum properties and 6 through 10 were assigned with piezoelectric properties. Each of the black dots represents a node and as can be seen, each of the elements is comprised of 8 nodes. After this 2D model was created, a 3D model was created using 8 noded elements as well. Figure 3.2 illustrates this, where only 4 nodes are visible from the side view and the remaining nodes are used in the creation of the width or depth of the model, as a minimum of 8 nodes are required to define a three dimensional hexahedral element. This 3D model was created for verification purposes only and another 3D model of different dimensions was used for the convergence study and optimization. Figure 3.2 shows the 3D cantilever beam model used for the convergence study and optimization. In accordance with the Euler-Bernoulli assumptions, the length is ten times larger than the width. The length of the beam is 2.5mm long, the width is 0.25mm wide, and each layer is 127μm thick, totaling 254μm in thickness. The PZT material overlays the aluminum section and covers the same amount of area and has the same thickness and therefore the same volume. It is clamped at one end while the other end is where the force is applied as a distributed force along the outer-most edge of the cantilever.

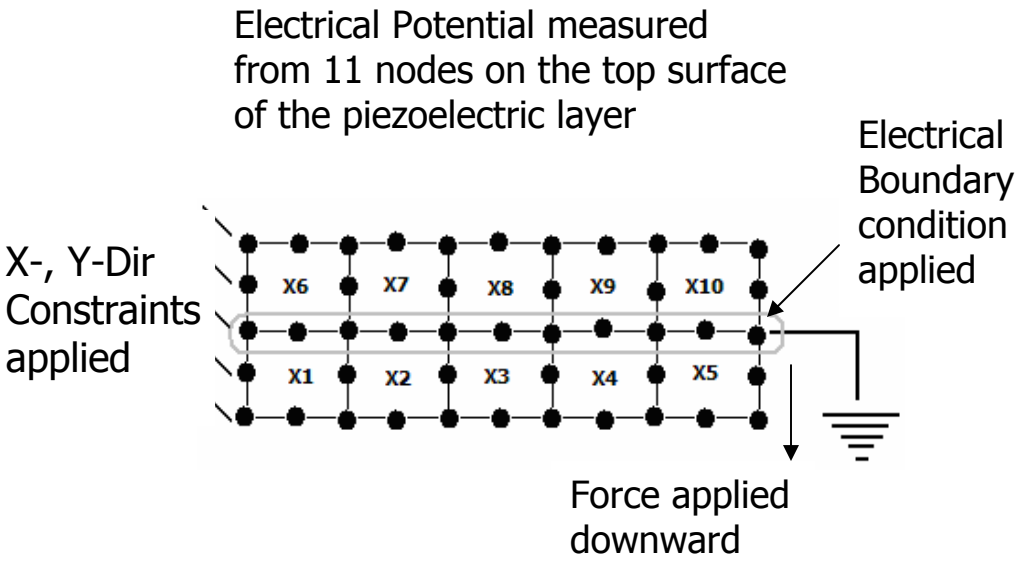

Figure 3.1: 2D Configuration

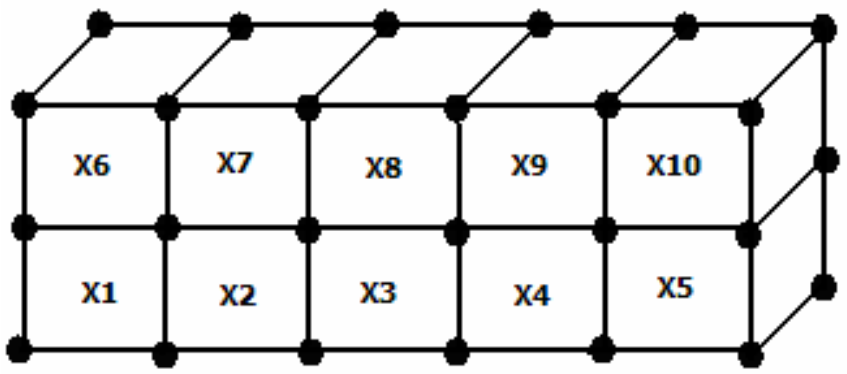

Figure 3.2: 3D Configuration

In the 3D model, nodes were created at points relative to the global co-ordinate system in such a way that 25 elements were created in each section of material, totaling 50 elements.

This was done in order to have a sufficiently fine mesh as determined by the convergence study without having the large computing costs associated with determining the field outputs requested such as strain, displacement, and most importantly, voltage. Figure 3.3 shows the full model of the microcantilever with the boundary conditions and end forces. Figure 3.4 shows a close up of the end forces. Only one element through the thickness of each material

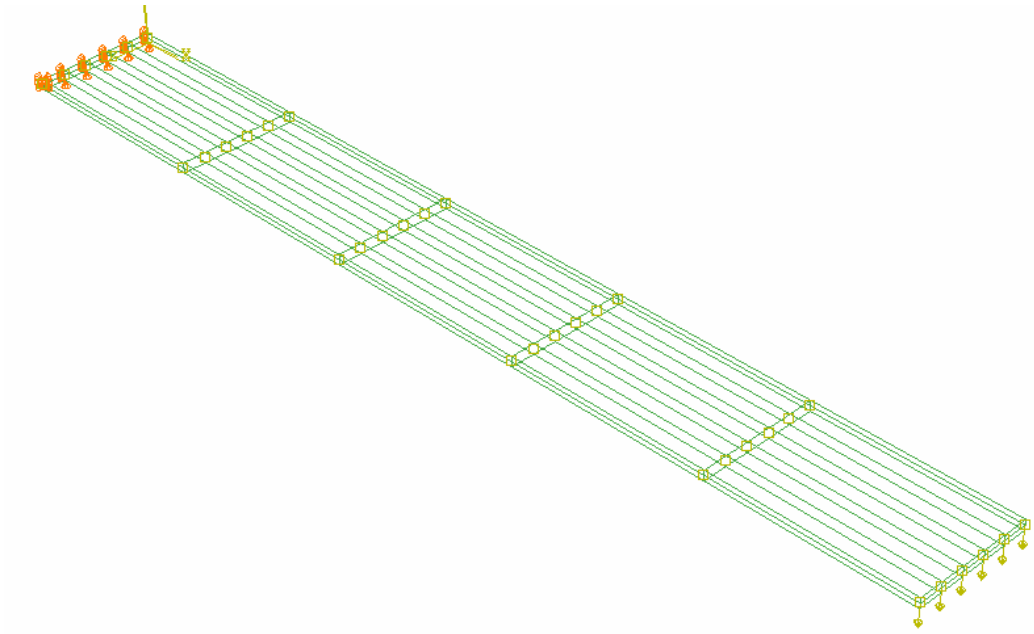

Figure 3.3: 3D Finite Element Model Used

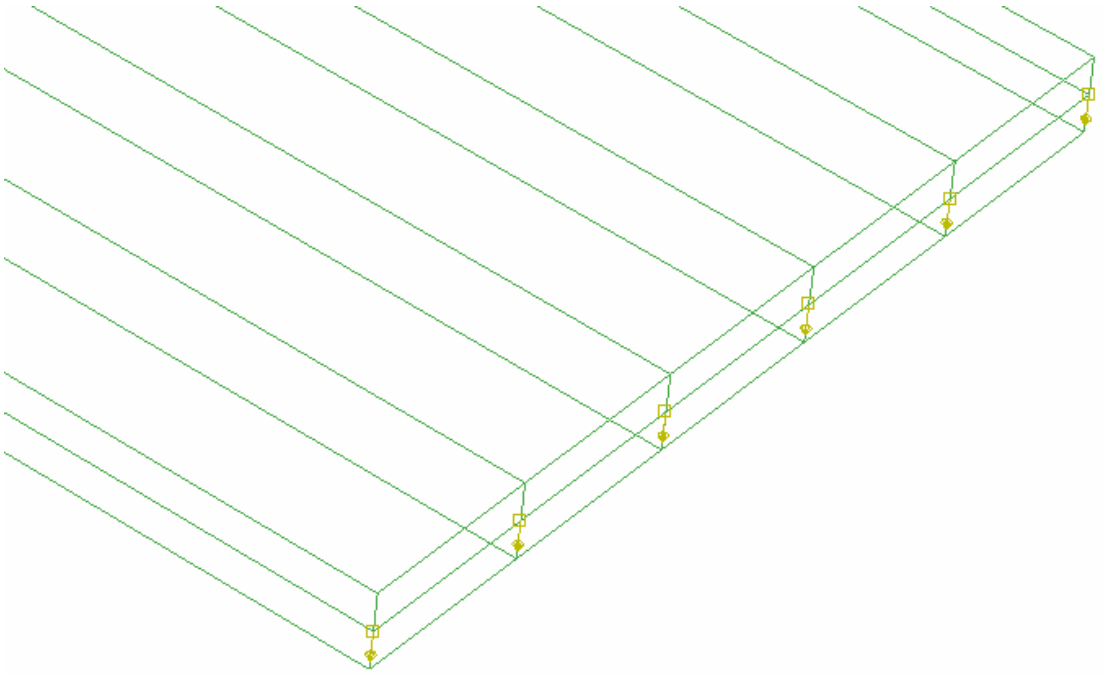

Figure 3.4: Close Up of Nodal End Forces

section was created as the strain varies linearly through the thickness of the beam; this further reduces the amount of computational time required. In addition, having separate elements provides the ability to assign different material properties to each element. This is critical for the optimization as our goal is to redistribute material to the volumes where there is a potential for greater voltage production, i.e. where the strain is largest.

3.1.1 BEAM ANALYTICAL MODEL

Figure 3.5 illustrates a typical cantilever beam setup. A cantilever beam is a structure whose length to width and/or thickness ratio is at least 10:1. This

means it is significantly longer than it is wide or thick. The beam developed here is 2.5mm long, 0.25mm wide, and 0.0254mm thick, where each layer has a thickness of 0.0127mm. One end of the beam is clamped down, i.e. no rotation or translation in any direction is permitted at this end and a tip force is applied to the free end acting perpendicular to the length of the beam at this point.

When the beam is subjected to a load, P, at the free end, the beam deflects and the curvature of the beam can be determined explicitly. The deflection of the free end is proportional to the magnitude of the load applied at this free end. A deflection caused by a tip force is demonstrated in figure 3.6.

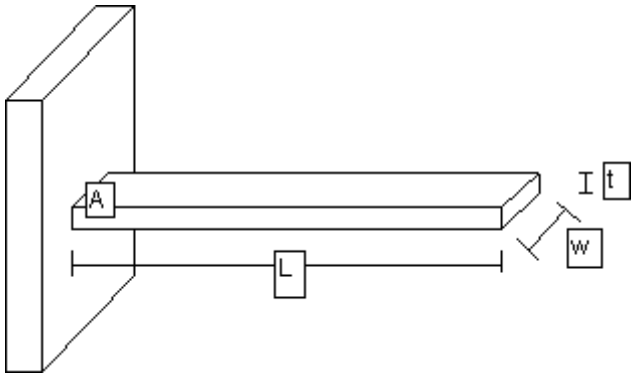

Figure 3.5: Typical Cantilever Beam Setup.

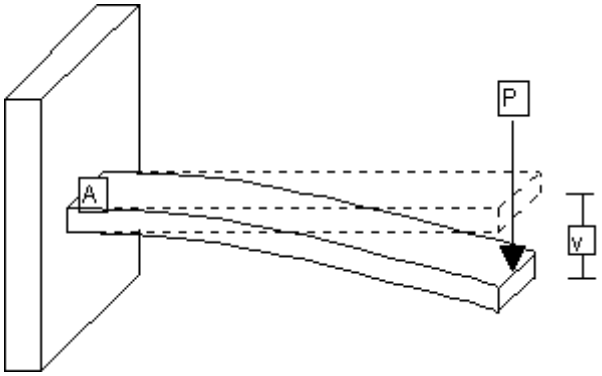

Figure 3.6: Cantilever Beam Tip Deflection Subject to a Tip Load

Equations have been developed that define the deflection of the tip exactly when the assumptions of small deflections and uniform beam cross sections are made. Small deflections equate to the material being subjected to loading in its linear elastic region. The curvature of the beam, κ, is equal to the second derivative of the deflection (Gere, 1997)

$$\kappa = \frac{\partial^2 \nu}{\partial \chi^2}$$

This curvature can be related to the bending moment, M, and the flexural rigidity, EI, as well where E is the elastic modulus of the beam and I is the moment of inertia.

$$\kappa = \frac{M}{EI}$$

The lateral loading on the beam, q, and the shear force, V, can both be related to the bending moment.

$$q = -EI\frac{\partial^4 \nu}{\partial \chi^4} \qquad V = EI\frac{\partial^3 \nu}{\partial \chi^3} \qquad M = EI\frac{\partial^2 \nu}{\partial \chi^2}$$

The load shown if Figure 3.4 defines the distributed load, the shear force, and the bending moment as follows:

$$q(x) = 0 \qquad V(x) = P \qquad M(x) = -PL(1 - \frac{x}{L})$$

Therefore the solution to the deflection at the free end can be determined by integrating along the length of the beam as follows:

$$\frac{\partial \nu}{\partial \chi} = \int_{x=0}^{x} M(x)dx = -\frac{PL}{EI}\left(x - \frac{x^2}{2L}\right)$$

$$\nu(x) = \int_{x=0}^{x} \frac{\partial \nu}{\partial x}dx = -\frac{PL}{EI}\left(\frac{x^2}{2} - \frac{x^3}{6L}\right)$$

$$\nu(L) = -\frac{PL^3}{3EI}$$

3.1.2 NATURAL FREQUENCY DETERMINATION

To find the modes of vibration and natural frequencies it would be easier to visualize a force applied and then removed from the tip. The beam would oscillate at a natural frequency unique to the beams geometry. This is dues to the inertia the beam has attained from being displaced by the tip force. Under the assumption of constant elastic modulus, inertia, and cross sectional area along the beams length, the equation for vibration is (Volterra, p. 310)

$$EI\frac{\partial^4 \nu(x,t)}{\partial x^4} = -\lambda_m \frac{\partial^2 \nu(x,t)}{\partial t^2}$$

Where the linear mass density of the beam is defined as

$$\lambda_m = \rho A$$

This differential equation of two variables, time and displacement, can be solved using separation of variables (Atkins, p.A29) assuming that the displacement can be divided into a part independent of time and the other independent of position.

$$\nu(x,t) = X(x)\,f(t)$$

Where X is time independent and f is position independent. Substitution into the beam equation then yields

$$EI\,\frac{\partial^4(X(x)\,f(t))}{\partial x^4} = -\lambda_m\,\frac{\partial^2(X(x)\,f(t))}{\partial t^2}$$

Or

$$\frac{EI}{\lambda_m X(x)}\frac{\partial^4 X(x)}{\partial x^4} = -\frac{1}{f(t)}\frac{\partial^2 f(t)}{\partial t^2}$$

This equation has been separated in such a way that the left side is time independent and the right side is position independent. This means that as time varies, the left side of the equation is a constant and similarly, as position varies, the right side is a constant. This constant can be denoted by the real quantity $\omega_n^{\,2}$ which denotes the natural frequencies of the beam. The beam equation can then be written in two parts (Volterra, p. 311):

$$\frac{\partial^4 X}{\partial x^4} - k_n^{\,4} X = 0 \qquad\qquad \frac{\partial^2 f}{\partial t^2} + \omega_n^{\,2} f = 0$$

Where

$$k_n{}^4 = \frac{\omega_n{}^2 \lambda_m}{EI}$$

3.1.3 ANALYTICAL MECHANICAL BOUNDARY CONDITIONS

A few initial conditions are required in order that this equation can be solved; these are determined by the boundary conditions applied to the beam. Being a cantilever beam, the fixed end has no translations and rotations, as well as no slope. In addition, the free end does not experience a bending moment or a shearing force.

Fixed End: $\nu(0,t) = X(0) = 0$ $\qquad \frac{\partial \nu(0,t)}{\partial x} = \frac{\partial X(0)}{\partial x} = 0$

Free End: $\frac{\partial^2 \nu(L,t)}{\partial x^2} = \frac{\partial^2 X(L)}{\partial x^2} = 0$ $\qquad \frac{\partial^2 \nu(L,t)}{\partial x^2} = \frac{\partial^2 X(L)}{\partial x^2} = 0$

3.1.4 CANTILEVER BEAM GENERAL SOLUTION

Volterra (p.312) defines the general solution to this beam equation with the applied boundary conditions as a linear combination of trigonometric equations:

$$X(x) = C_1\left[\cos(k_n x) + \cosh(k_n x)\right] + C_2\left[\cos(k_n x) - \cosh(k_n x)\right]$$

$$+ C_3\left[\sin(k_n x) + \sinh(k_n x)\right] + C_4\left[\sin(k_n x) - \sinh(k_n x)\right]$$

The first boundary condition enables C_1 to be determined:

$$X(0) = 0 = C_1[2] \qquad C_1 = 0$$

Taking the derivative of the general solution and applying the second boundary condition yields C_3:

$$\frac{\partial X(x)}{\partial x} = C_2[-\sin(k_n x) - \sinh(k_n x)]$$
$$+ C_3\left[\cos(k_n x) + \cosh(k_n x)\right] + C_4\left[\cos(k_n x) - \cosh(k_n x)\right]$$

$$\frac{\partial X(0)}{\partial x} = 0 = C_3[2] \qquad C_3 = 0$$

Taking the second and third derivatives of the general solution leads to two simultaneous equations which when solved yield C_2 and C_4 as follows:

$$\frac{\partial^2 X(L)}{\partial x^2} = C_2\left[-\cos(k_n L) - \cosh(k_n L)\right] + C_4\left[-\sin(k_n L) - \sinh(k_n L)\right] = 0$$

$$\frac{\partial^3 X(L)}{\partial x^3} = C_2\left[\sin(k_n L) - \sinh(k_n L)\right] + C_4\left[-\cos(k_n L) - \cosh(k_n L)\right] = 0$$

$$C_4 = C_2\left\{\left[\cos(k_n x) - \cosh(k_n x)\right] + \frac{\left[-\cos(k_n x) - \cosh(k_n x)\right]}{\left[\sin(k_n x) - \sinh(k_n x)\right]}\left[\sin(k_n x) - \sinh(k_n x)\right]\right\}$$

$$C_4 = C_2\frac{\left[-\cos(k_n L) - \cosh(k_n L)\right]}{\left[\sin(k_n L) + \sinh(k_n L)\right]}$$

The general solution can then be reduced with the proper substitutions as follows:

$$X_n(x) = C_2\left\{C_3\left[\cos(k_n x) - \cosh(k_n x)\right] + \frac{\left[-\cos(k_n L) - \cosh(k_n L)\right]}{\left[\sin(k_n L) - \sinh(k_n L)\right]}\left[\sin(k_n x) - \sinh(k_n x)\right]\right\}$$

Volterra (p. 312) states that C_2 is arbitrary but as the target is for the dynamic solution to equate the static solution at time = 0, C_2 must equal 0.5, leading to

$$X(0) = 0 \qquad \text{and} \qquad X(L) = 1$$

This then yields the equation to determine the natural frequencies of the cantilever beam:

$$\cos(k_n L)\cosh(k_n L) = -1$$

The solutions for the constants k_nL give the natural frequencies of the beam, where k_n is related to the elastic modulus, inertia, density, and cross sectional area of the beam:

$$k_n = \sqrt{\frac{\rho A \omega_n}{EI}}$$

Where w_n is the n^{th} natural frequency of the beam. Figure 3.7 illustrates the various mode shapes for a cantilevered beam.

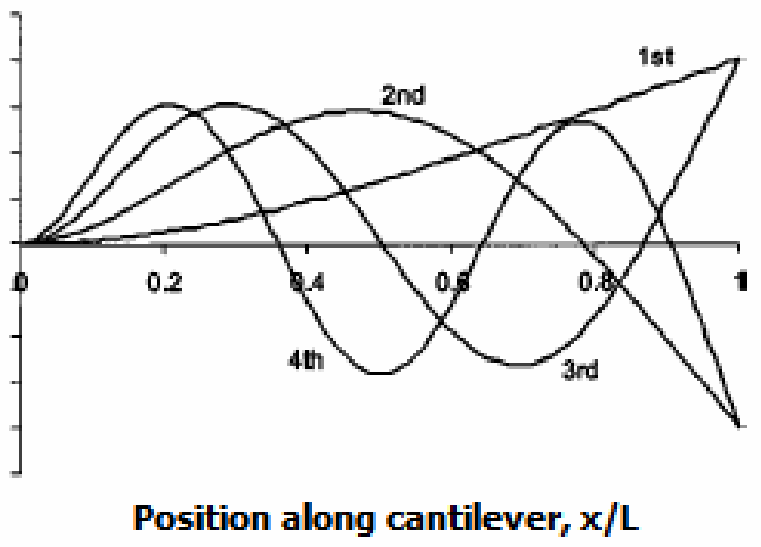

Figure 3.7: Mode Shapes for a Cantilever Beam in Free Vibration

(Thundat et. al. 1997)

3.1.5 STEPS AND LOADS

The first step defined in the model determines the first few natural frequencies of the beam. This provides the chance to determine a suitable vibration source for the beam under dynamic loading. Depending on what the input vibration frequency is, the power generation capability can be determined relative to how close to one of the natural frequencies the source is. ABAQUS has the capacity to determine these natural frequencies. The analytical values for the natural frequencies as determined using the Euler-Bernoulli approach are presented in table 3.1.

Table 3.1: Analytical Natural Frequencies for the Modeled beam

Hz	**Analytical**
w_{n1}	255.37
w_{n2}	1598.7
w_{n3}	2878.3

3.2 OPTIMIZATION MODEL

The objective in the optimization model is setup to maximize voltage. It can be written as follows:

Maximize ΣV_i (Voltage)

ΣV_i **i = 1…n (number of nodes)**

Subject to

$$\mathbf{1E\text{-}5 \leq X \leq 1.0}$$

Where V represents the summation of the voltages produced on the top 36 nodes (n) of the finite element model in the piezoelectric layer and X represents the material fraction of each individual element. There are 36 nodes on the top most surface of the piezoelectric layer, where the strain due to the tip deflection is greatest. It is this summation of the nodal voltages produced at these 36 nodes which are defined in the optimization model as the objective. There are 50 design variables in the model. These are defined as being the individual material fractions in each of the 50 elements. The only constraints applied are lower and upper bounds is placed on the values that each material fraction can be. A lower bound of 1E-5 prevents singularities in the stiffness matrix which ideally would

mean there is no material in the corresponding element. An upper bound of 1.0 corresponds to the element having full material. A commercial FORTRAN code named NLPQL is used for the optimization model.

The goal is to edit the individual material properties of each defined element in both the PZT and Aluminum layers, with the maximization of voltage produced being the desired result.

The individual material properties are assigned to each element according to their material fraction. In order to maintain uniformity in each element, the principles of homogenization were applied. This is where a void is assumed in the discretized material element. This void is essentially assumed to be separated in infinitely smaller voids within the element, resulting in uniformly homogeneous material properties throughout each element.

Figure 3.8 demonstrates how homogenization can be viewed. If voids are introduced to finite elements, the equivalent overall density and material properties can then be evaluated and the new material cell can be defined.

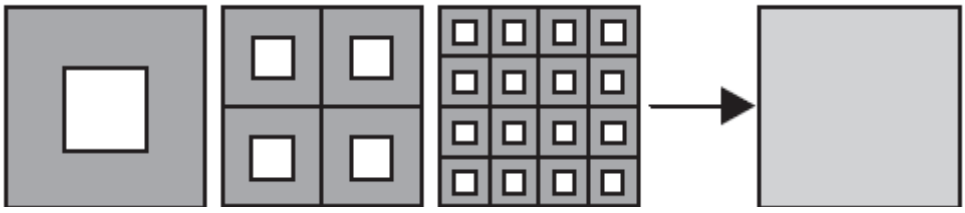

Figure 3.8: Illustration of the Homogenization Process

3.2.1 FORTRAN MODEL

NLPQL operates on the basis that numerical gradients at each iteration of the step is calculated numerically using the finite difference method. This leads the objective function in the direction leading to a maximum.

First, a list of material fractions at an initial starting point was made; Zero material fraction indicates a void whereas a material fraction of 1 signifies full material occupation of the respective element. Next, a program was developed that determined the material properties that need to be written into the input file according to what the material fraction is. These properties are listed in table 3.2. Aluminum has only isotropic elastic modulus and density, whereas PZT has orthotropic modulus of elasticity, isotropic dielectric stress constant, isotropic coupling coefficient, and density. The relationship for elastic moduli with respect to material fraction is presented in figure 3.8. This was developed in a homogenization study performed on PSI-5H4E, as type of piezoelectric material. The three plots include E11, E12, and E66, which represent the main diagonal, the off diagonal, and the shear elastic moduli of the piezoelectric material.

Of the properties listed for both materials, only density is linearly proportional to the material fraction. These relationships adopted into determining the values that are required in the model input file to be read by ABAQUS.

In addition, relationships for the coupling coefficients were adopted to be used in determining the values to be used for the ABAQUS input file. These relationships are presented in figures 3.9 and 3.10.

Table 3.2: Model Material Properties.

	Aluminum	Piezoelectric
Modulus - E (Gpa)	71	62
Density - ρ(Kg/m3)	2700	7800
Poisson's Ratio	0.33	0.35
Dielectric Constant		3800
Piezoelectric Coupling g_{31} (C/m^2)		-4.5
Piezoelectric Coupling g_{33} (C/m^2)		19

Once these relationships between material fraction and material properties were established for both the PZT and Aluminum, another code was developed in FORTRAN that writes these material properties to the input file. At this point, an ABAQUS job is initiated to determine the voltage production at the top most surface of the PZT section, namely from 36 nodes. Next, another FORTRAN program was written to read the voltages produced at these top surface nodes and add them up.

Bounds are also placed on the material fraction, where an upper bound of 1 signifies 100% material occupying a defined element and 1E-5 represents a void. 1E-5 was chosen as the lower bound to avoid singularities in the stiffness matrices. And from a manufacturing point of view was done to ensure a continuous substrate layer, where voids are undesirable because of the difficult of manufacturability in addition to the possibility of concentrated stress regions being developed.

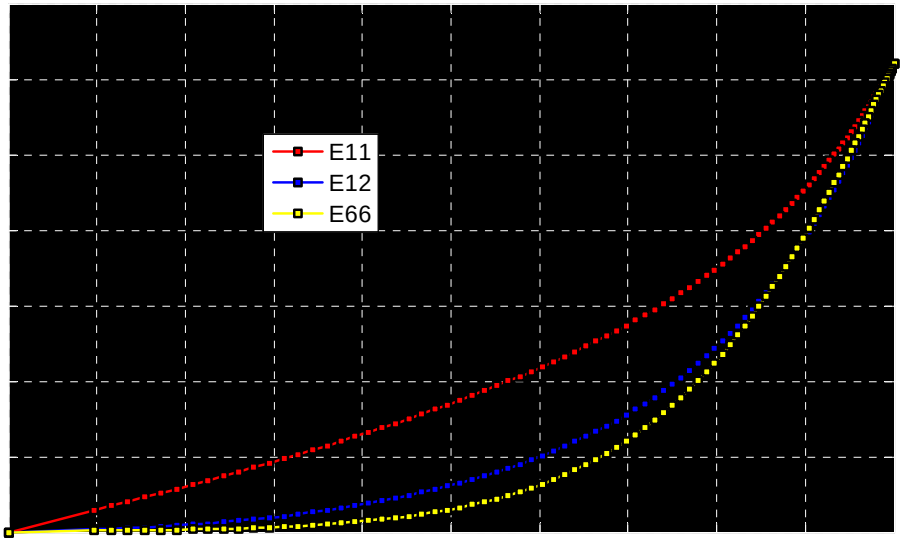

Figure 3.9: Variation of Piezoelectric Elastic Moduli w.r.t. Material Fraction

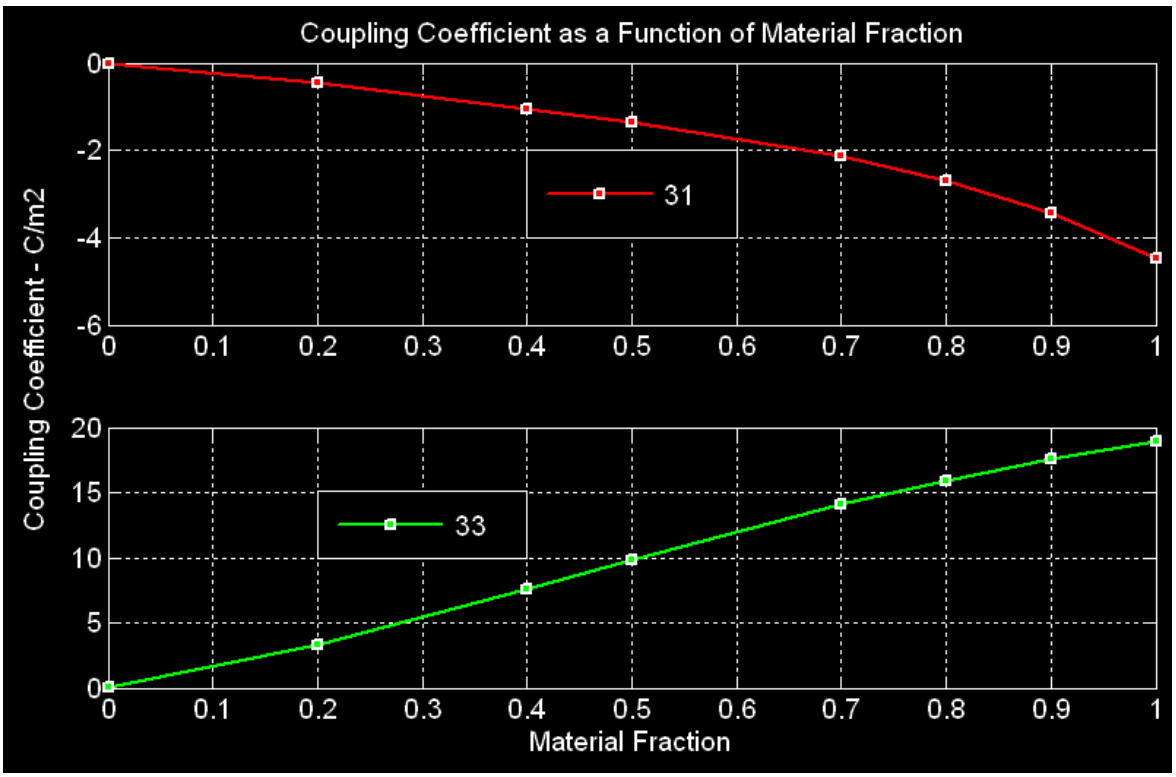

Figure 3.10: Variation of Coupling Coefficients w.r.t. Material Fraction

In addition, symmetry was applied to the design variables as the beam is perfectly symmetrical along its length, where even the load is symmetrically applied at the free end.

Once these increments are added or subtracted, the new material properties are determined based off these new material fractions, which are then re-written into the input file to be read by ABAQUS once again. This yields a new set of electrical potentials on the top most surface of the PZT which then get summed up. If this sum is greater than the previously determined voltage sum, the optimization code continues subtracting or adding material fractions in the same fashion, otherwise different gradients are calculated and material is redistributed into other volumes of the beam until all directions have been exhausted and no other feasible combinations of material fractions yield a higher voltage sum.

An illustration of the optimization is presented in chart form in figure 3.11 and figure 3.12 shows how the symmetry conditions were applied.

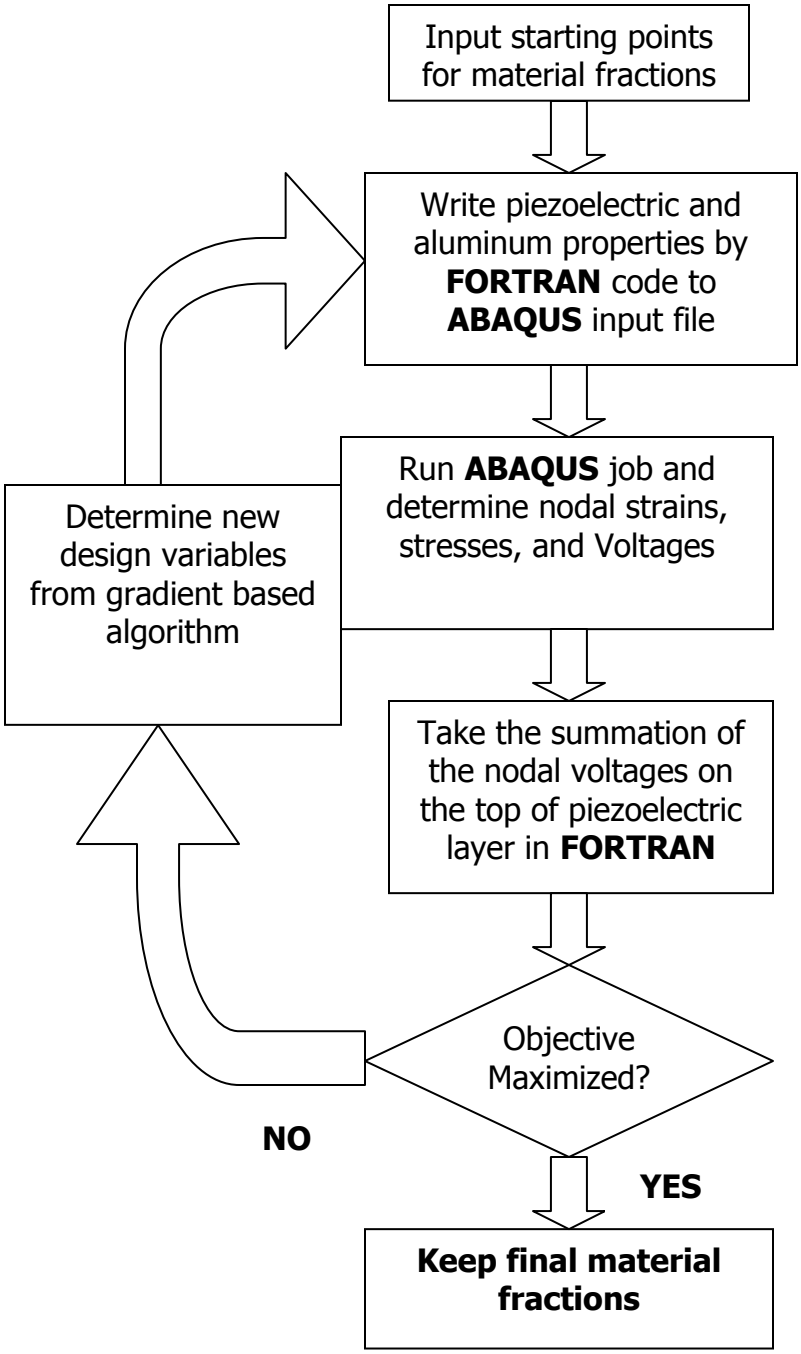

Figure 3.11: Illustration of the optimization process.

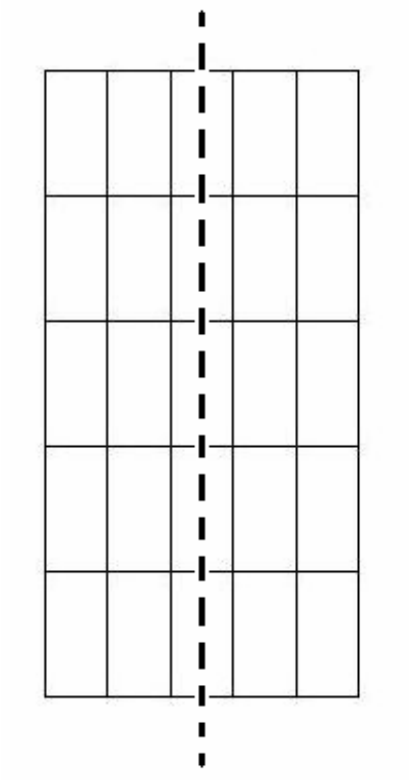

XL XR

Figure 3.12: Illustration of the Symmetry in the Cantilever Model

First, a starting point for all the elements is given. They can be assigned any values between 1E-5 and 1. Once this is done, the FORTRAN code is compiled and the ABAQUS input file is written to with new material properties for each finite element as described by the material relationships with respect to material fraction in figures 3.8 and 3.9. An ABAQUS job is then run where field output results include the nodal quantities stress, strain, and Voltage. These values are then read for the appropriate nodes on the top surface of the piezoelectric material and the objective function is determined. This process is continued until

the KKT conditions of the optimization process are met, in which case the optimization process is assumed to have converged on a solution.

CHAPTER 4: RESULTS

4.1 FINITE ELEMENT RESULTS

4.1.1 3D MODEL VERIFICATION

Electrical potentials along the top surface of the 3D model were summed and compared to the summation of the nodal electric potentials on the top surface of the 2D model. In addition, the tip displacements were compared for the same end force. This was conducted between a range of frequencies, where an iterative process was carried out to find a suitable range around the first natural frequency of the beam. An arbitrary damping ratio of 0.1 was applied to the model to prevent singularities when the beam was excited at the natural frequency. The results are presented in figure 4.1 and as can be seen, the 2D and 3D model results overlay each other perfectly, indicating that the 3D model is accurate.

4.1.2 ELEMENT CONVERGENCE STUDY

Computational expense was a criterion crucial to this study. Too many elements and the job would take too long to process without giving significant increase in accuracy of the results. This was especially important in the optimization process. The number of feasible search direction iterations increases exponentially with an increase in number of elements. A convergence study was carried out to determine a suitable cutoff. The figures 4.2, 4.3, and 4.4 illustrate the convergence of the first 3 natural frequencies of the model.

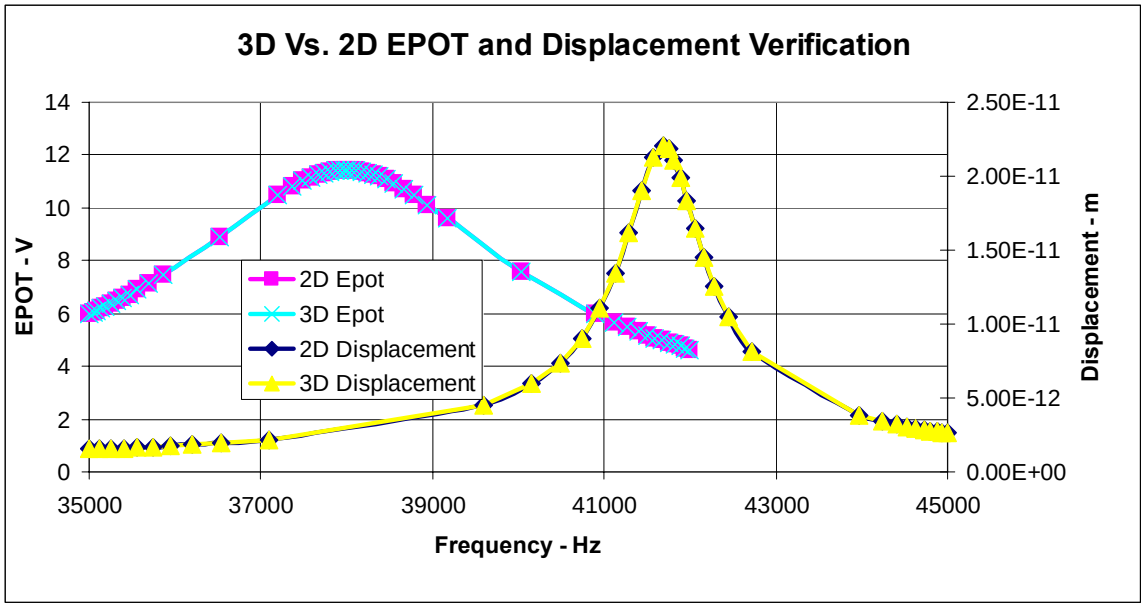

Figure 4.1: 3D Model Verification

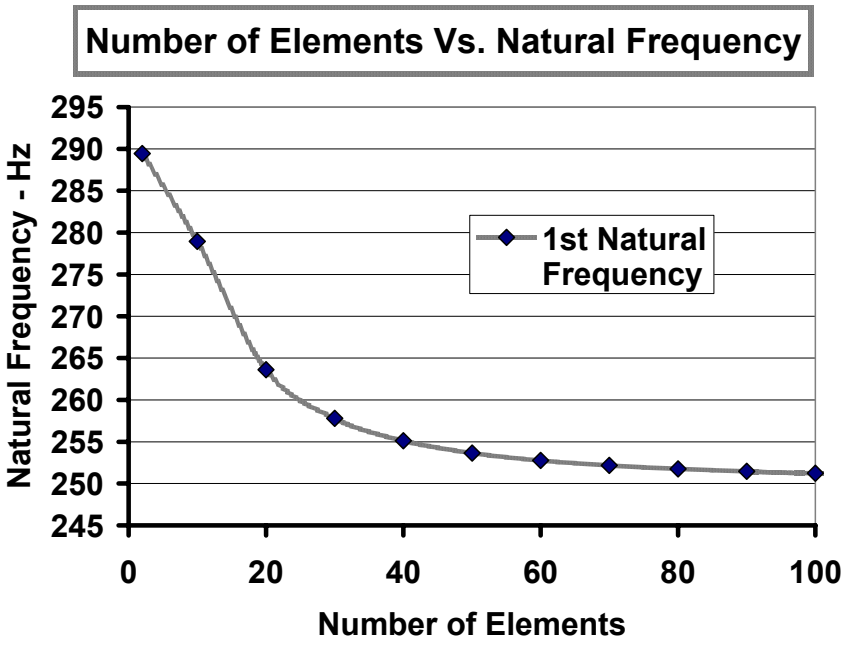

Figure 4.2: Convergence study for the 1st Natural Frequency Vs. Number of Elements

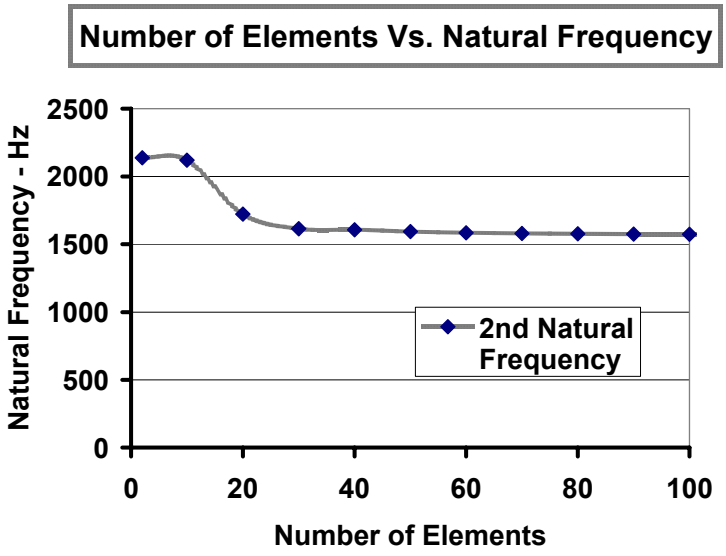

Figure 4.3: Convergence study for the 2nd Natural Frequency Vs. Number of Elements

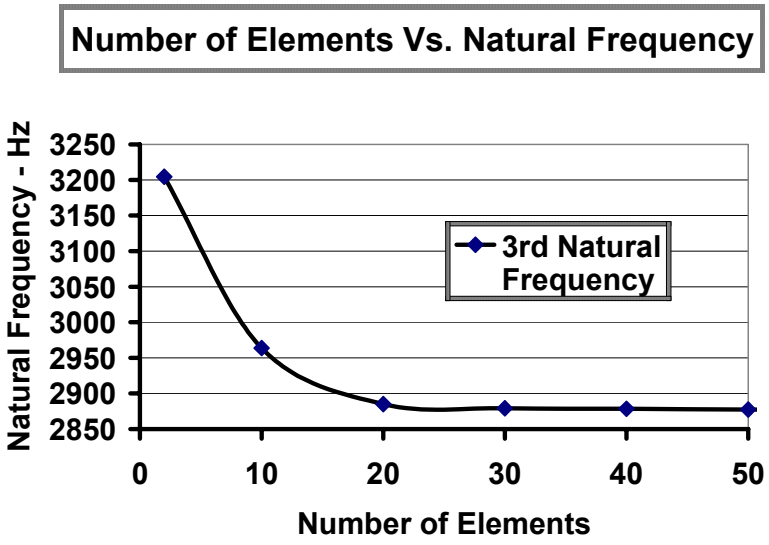

Figure 4.4: Convergence study for the 3rd Natural Frequency Vs. Number of Elements

From these figures, it can be seen that 50 elements is a suitable number of elements, where there is no significant gain in accuracy with any greater number of elements.

The determining factor was pretty much the first natural frequency. Approximately 20 elements is a suitable cutoff for the second and third natural frequencies.

4.1.3 NATURAL FREQUENCY VERIFICATION

The natural frequencies of the beam were also verified. Using the beam characteristic equations, the first 3 natural frequencies were determined and compared to the output results from the 50 element ABAQUS model. This is presented in table 4.1. An equivalent elastic stiffness is used incorporating the two different elastic moduli of the materials constituting the microcantilever. After finding the distance to the neutral axis using standard mechanics of materials approach, the equivalent inertia of the beam is found. Using these equivalent values, the natural frequency was determined analytically.

Table 4.1: Natural Frequency Verification

	Analytical	ABAQUS	% Error
w_{n1}	255.37	253.65	0.673533
w_{n2}	1598.7	1592.9	0.362795
w_{n3}	2878.3	2877.3	0.034743

4.2 OPTIMIZATION RESULTS

A presentation of the optimization results is given here. Various starting points and their graphical illustration are given. The microcantilever beam measures 2.5mm long, 0.25mm wide, and 254μm thick, where each layer has a thickness of 127μm and a static load of 1μN is placed at the tip, which is distributed evenly among the 6 nodes at the free end as illustrated in figure 3.4.

4.2.1 DIFFERENT STARTING POINTS

The two rectangles presented next to each other in the next set of figures represent the two layers of the microcantilever, where the left layer represents the piezoelectric material, and the right one represents the aluminum layer. The top of the figures is where the mechanical boundary conditions are applied, or essentially, where the beam is clamped. The lower end of the figure is where the tip load is placed. 1E-5, the lower bound on the material fractions, 0.1, 0.25, 0.5, 0.75, and 1.0 were some of the initial material fractions used as starting points. In addition, 100% piezoelectric and 1E-5 aluminum starting material fractions were used. This is presented in figures 4.5-4.10 and figures 4.11 and 4.12 show a max/min and a tapered case. Intuitively, the expected results were a tapered or faded topology, where the least amount of aluminum is expected near the boundary conditions to maximize strain and the most near the end to maximize deflection, analogous to an end mass. Similarly, an inverse taper is expected in the piezoelectric layer, where most of the material is expected to be accumulated

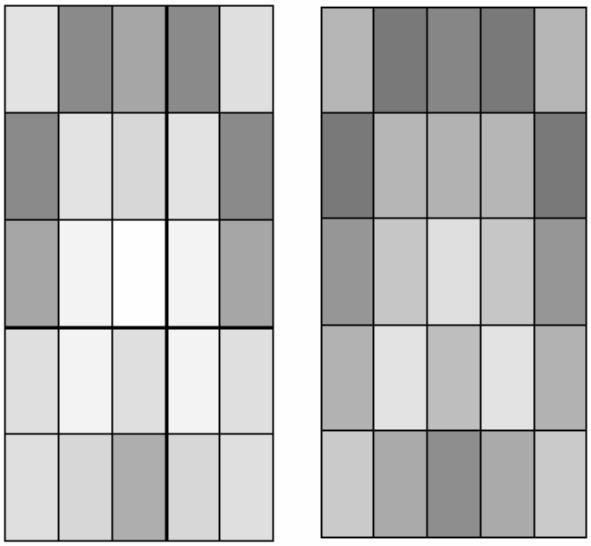

Figure 4.5: 1E-5 Initial Material Fraction for all elements

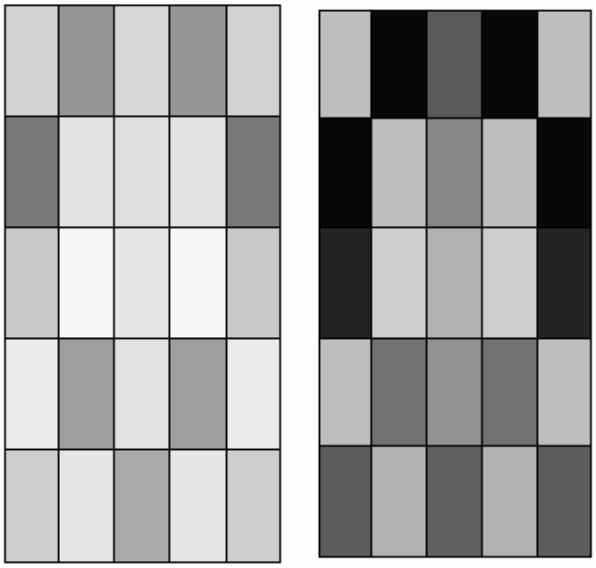

Figure 4.6: 0.1 Initial Material Fraction for all elements

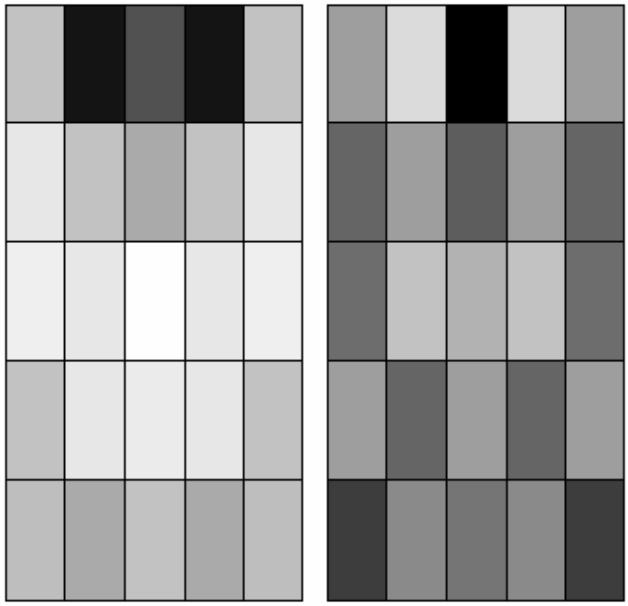

Figure 4.7: 0.25 Initial Material Fraction for all elements

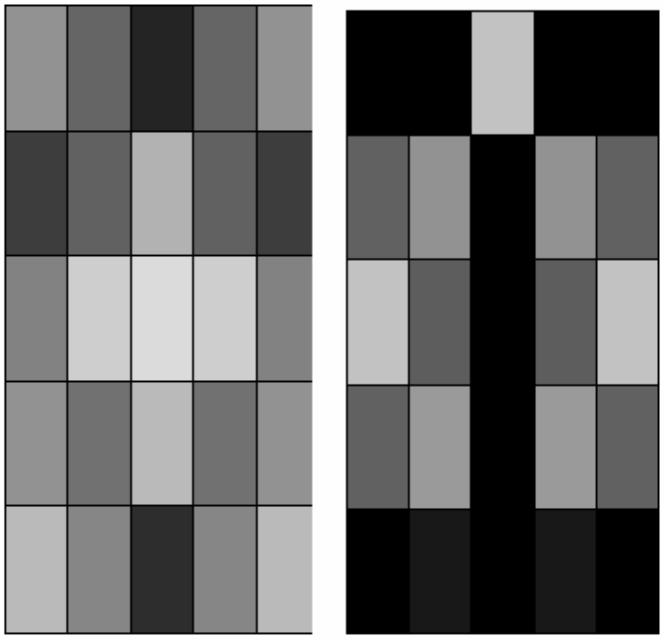

Figure 4.8: 0.5 Initial Material Fraction for all elements

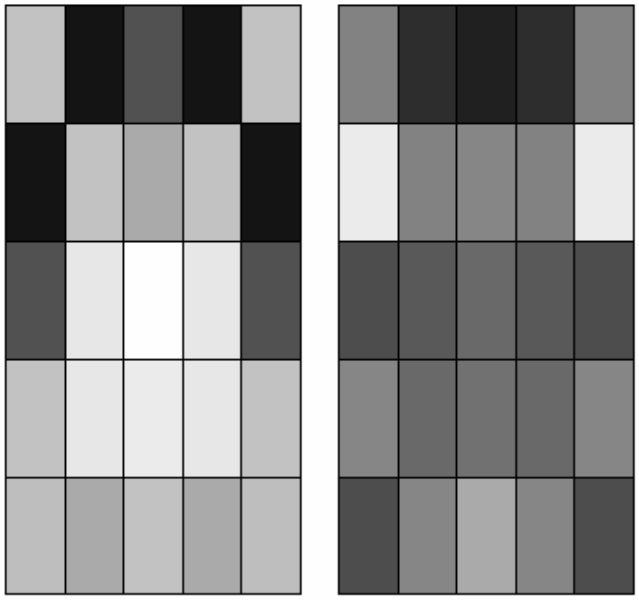

Figure 4.9: 0.75 Initial Material Faction for all elements

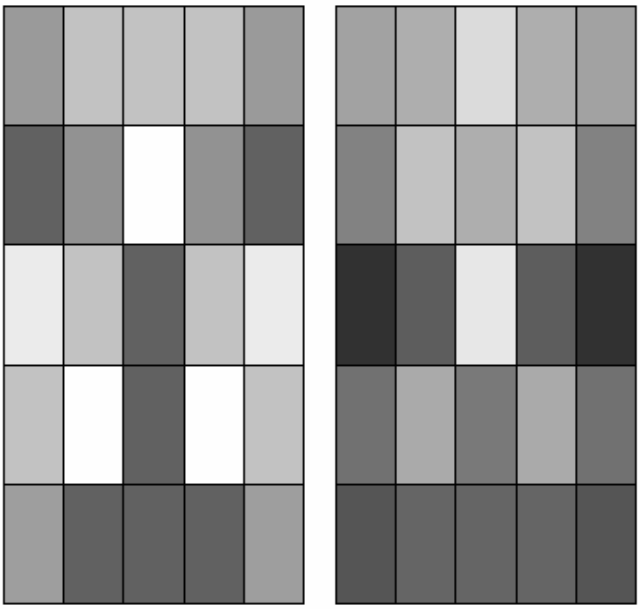

Figure 4.10: 1.0 Initial Material Fraction for all elements

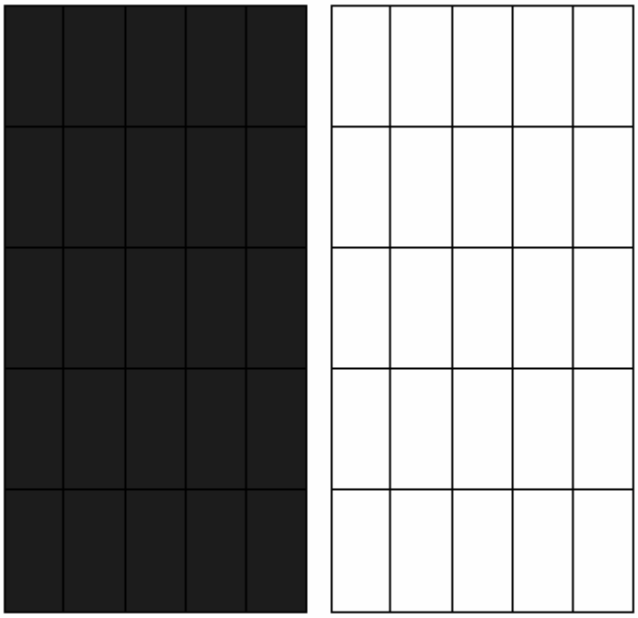

Figure 4.11: 1.0 Material Fraction for Piezoelectric and 1E-5 for Aluminum

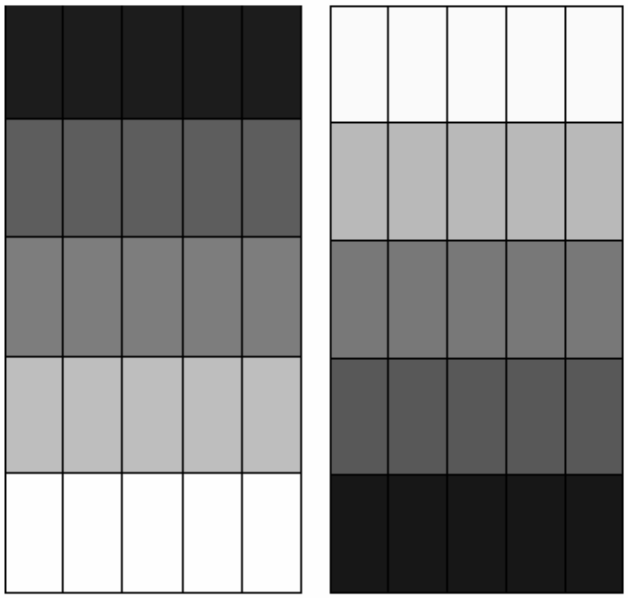

Figure 4.12: "Tapered" Initial Material Fractions

Table 4.2: Starting Material Fractions and Final Optimization Objective Function Values.

Starting Material Fractions	Final Function Value
1.00E-05	-8.02
0.1	-3.96E+05
0.25	-2.39E+06
0.5	-1.36E+08
0.75	-3.20E+05
1	-1.19E+04
Full Piezo Least Aluminum	-2.54E-01
Tapered	-3.70E+05

near the boundary condition, where the greatest strain is, and conversely the greatest electric potential is produced, and less material towards the tip force, or free end of the cantilever beam, where the least strain and conversely the least voltage is produced. Table 4.2 lists the starting material fractions and final optimization objective function values and table 4.3 shows nodal deflections for four different initial starting points. The nodes listed are all the nodes on the vertical plane of the free end of the microcantilever beam.

F(X) in the table above indicates the objective function value. As shown in table 4.3, the optimal case occurs when the initial material fractions are 0.5 or 50%. This is indicative of several final results which is highly dependant on the initial conditions on the material fractions.

Table 4.3: Nodal Deflections for 4 different initial Material Fractions.

	Tapered	100% Piezo Min. Aluminum	Optimal	50% Piezo 50% Alum
NODE	**U2 (meters)**	**U2 (meters)**	**U2 (meters)**	**U2 (meters)**
1	-8.546E-06	-2.619E-08	-9.717E-06	-9.691E-08
2	-8.546E-06	-2.619E-08	-9.717E-06	-9.691E-08
3	-1.136E-01	-3.480E-04	-1.291E-01	-1.288E-03
4	-1.136E-01	-3.480E-04	-1.291E-01	-1.288E-03
9	-5.678E-02	-1.740E-04	-6.456E-02	-6.439E-04
10	-5.678E-02	-1.740E-04	-6.456E-02	-6.439E-04
13	-8.546E-06	-2.619E-08	-9.717E-06	-9.691E-08
14	-8.546E-06	-2.619E-08	-9.717E-06	-9.691E-08
15	-8.546E-06	-2.619E-08	-9.717E-06	-9.691E-08
16	-8.546E-06	-2.619E-08	-9.717E-06	-9.691E-08
17	-1.136E-01	-3.480E-04	-1.291E-01	-1.288E-03
18	-1.136E-01	-3.480E-04	-1.291E-01	-1.288E-03
19	-1.136E-01	-3.480E-04	-1.291E-01	-1.288E-03
20	-1.136E-01	-3.480E-04	-1.291E-01	-1.288E-03
45	-5.678E-02	-1.740E-04	-6.456E-02	-6.439E-04
46	-5.678E-02	-1.740E-04	-6.456E-02	-6.439E-04
47	-5.678E-02	-1.740E-04	-6.456E-02	-6.439E-04
48	-5.678E-02	-1.740E-04	-6.456E-02	-6.439E-04
F(X)	**-370000**	**-0.254**	**-136000000**	**-251713.55**

Table 4.3 shows the nodal deflections on the surface of the free end. The optimal case is where the initial material fractions are 0.5; this yields the greatest function value and also has the greatest deflection of any of the other cases. Nodes 1, 2, 13, 14, 15, and 16 lie on the central plane of the bi-layer. Nodes 9, 10, 45, 46, 47, and 18 lie on the top edge of the free end or 127μm, equivalent to the thickness of the piezoelectric layer, above the central plane. Nodes 3, 4, 17, 18, 19, and 20 lie on the bottom edge of the free end or 127μm, equivalent to the thickness of the aluminum layer, beneath the central plane. The deflections are in S.I. units of meters and since the cantilever beam is 2.5mm long, are unrealistic.

In a harvesting circuit, a typical resistor used can have a resistance of 100KΩ (Umeda et. al., 1997). The objective function value, indicative of the nodal voltages produced, when divided among the total number of nodes can be used to determine the power values as shown:

Total Voltage: 136,000,000 V

Scaled Voltage: $\frac{136,000,000}{1E6} = 136\,\text{V}$

Voltage per node: $\frac{136V}{36nodes} = 3.78V$

Power: $P = \frac{V^2}{R} = \frac{3.78^2}{100K\Omega} = 0.14mW$

A scaled voltage is introduced as the objective function value, or voltage, is directly related to the magnitude of the tip force. By scaling it down to 1μN, a more reasonable electric potential is realized at the nodes. The power levels shown are very promising, especially when taking an array vantage point, where potentially hundreds of microcantilevers can be arranged to function as a synonymous system.

The optimal shape as shown in figure 4.8 does not have a very uniform distribution of material. This may be extremely difficult to fabricate. However, an alternate approach would be to drive the material fractions which are close to 1.0 to 100% and similarly the ones which are close to 1E-5 to 0%, as long as this does not create an obscure looking shape that would be highly un-manufacturable. In addition, a study would have to be done into the voltage

produced from this manufacturable topology to ensure that it is in line with the goal of maximizing voltage production.

5. CONCLUSIONS AND MODEL ENHANCEMENTS

In this thesis the aim was to create a finite element model of a piezoelectric and aluminum bi-layer cantilever beam, evaluate its natural frequencies, determine the stresses and stains, and obtain the nodal voltages. In addition, it was attempted to optimize the topology of the beam in order to maximize the voltage produced from the strain in the piezoelectric material. Not only were the finite element capabilities for determining the natural frequencies reaffirmed but an optimized model was seen that followed an expected tapered design.

From the analysis performed in this research, some conclusions can be made.

A model that predicts voltage generation from an externally induced deflection on the free end of the beam has been developed. The model accurately predicts the natural frequency. Ideally, the force used to excite the beam could be arbitrary in nature.

To obtain accurate estimations of power generation, the damping ratio should be well estimated in order to utilize a vibrating source of excitation

The transverse force location is optimal at the free end of the cantilever beam, producing the largest moment arm. Damping plays a critical role when predicting power from piezoelectric MEMS models. Ideally, the damping ratio would be known to ensure precise and accurate results. Oftentimes, a way of determining the damping ratio involves performing log decrement analyses or frequency response calculations. The purpose of this research is to develop a model that can be built on so that it could be possible to accurately determine and design a

working device that can be geared to operate in an arbitrary environment with little enhancing to accommodate it in its specific application. This can be somewhat limited by environmental damping, which is significant on the micro scale.

From the study done in this research, some of the items to be looked at in future work include a continuation of this analytical model that predicts the power generation for any arbitrary forcing function. An force in the form of an impact or one that is discrete with respect to time, are realistic forms of forces and could affect the impact of power generation.

A method to accurately estimate the damping for these models should be investigated. Damping for a structure needs to be well estimated before using the models to predict power generation.

An interactive, user-friendly interface that would allow the user to input dimensions, parameters, and properties of a system could be developed in a software code to allow ease and efficiency of use. This would make it simple for someone who is not familiar to the specific software code and could reduce input errors by explicitly altering the software code.

A model that adequately predicts power generation for arbitrary substrate shapes can then be developed. Plates, disks, and beams are shapes that have potential in industry depending on the specific application.

Next, the electrical harvesting of the generated power needs to be examined. This includes understanding and developing adequate voltage regulators,

choosing the proper capacitors, and optimizing the resistors in an energy harvesting circuit to optimize energy reclamation.

Also, depending on the source of vibration, a suitable application can be determined and though the power produced may not be large in quantity, over time this stored energy can be significant enough to be used intermittently in devices where it may be needed.

Additional items for consideration are scalability of the microcantilevers which makes a large array for a compounded result. The effects of electrical leakage in the system needs to be considered as well as does the response to random vibrations, and not just in the vicinity of natural frequencies.

BIBLIOGRAPHY

BIBLIOGRAPHY

Atkins, P. W. Physical Chemistry. 5th ed. New York: W. H. Freeman and Company, 1994.

Gere, J. M., Timoshenko, S. P. Mechanics of Materials. 4th ed. Boston: PWS Publishing Company, 1997, pg. 602.

Voltera, E., Zachmanoglou, E. C. Dynamics of Vibrations. Columbus, Charles E. Merrill Books, Inc., 1965.

Sodano,HA,Inman,DJ, Park G, 'Comparison of piezoelectric energy harvesting devices for recharging batteries', Journal Of Intelligent Material Systems And Structures Vol. 16 (10): OCT 2005, pg. pg. 799-807.

Buehler MJ, Bettig B, Parker GG, 'Topology optimization of smart structures using a homogenization approach', Journal Of Intelligent Material Systems And Structures Vol. 15 (8): AUG 2004, pg. pg. 655-667.

Wang ZY, Yue RF, Zhang RX, et al. 'Design And Optimization Of Laminated Piezoresistive Microcantilever Sensors', Sensors And Actuators A-Physical Vol. 120 (2): May 17 2005, pg. pg. 325-336

duToit NE, Wardle BL, Kim SG, 'Design considerations for MEMS-scale piezoelectric mechanical vibration energy harvesters', Integrated Ferroelectrics Vol. 71, 2005, pg. 121-160.

Sodano HA, Park G, Inman DJ. 'Estimation Of Electric Charge Output For Piezoelectric Energy Harvesting', Strain, Vol. 40 (2), May 2004, pg. 49-58.

Dareing DW, Tian F, Thundat T 'Effective Mass And Flow Patterns Of Fluids Surrounding Microcantilevers' Ultramicroscopy Vol. 106 (8-9), Jun-Jul. 2006, pg. pg. 789-794.

Dareing DW, Thundat T, Jeon SM, et al. 'Modal analysis of microcantilever sensors with environmental damping', Journal Of Applied Physics Vol. 97 (8), APR 15 2005 Art. No. 084902.

Thundat T, Oden PI, Warmack RJ, 'Microcantilever Sensors', Microscale Thermophysical Engineering Vol. 1 (3), JUL-SEP 1997, pg. 185-199.

Elvin NG, Elvin AA, Spector M, 'A Self-Powered Mechanical Strain Energy Sensor', Smart Materials & Structures Vol. 10 (2), APR 2001 pg. 293-299.

Elvin N, Elvin A, Choi DH, 'A Self-Powered Damage Detection Sensor', Journal Of Strain Analysis For Engineering Design, Vol. 38 (2), pg 115-124.

T. Douseki, 'A Batteryless Optical-Wireless System with White-LED Illumination', Personal, Indoor and Mobile Radio Communications, 2004, pp. 2529-2533.

S. Meninger, J. O. Mur-Miranda, R. Amirtherajah, A. P., Chandrakasan, J. H. Lang, 'Vibration-to-Electric Energy Conversion', IEEE Transactions on Very Large Scale Integration (VLSI) Systems, vol. 9, no. 1, 2001, pg. 64-75,.

Gere, J. M., Timoshenko, S. P. Mechanics of Materials. 4th ed. Boston: PWS Publishing Company, 1997.

Amirtharajah, R., Chandrakasan, A. P. 'Self-powered Signal Processing Using Vibration-based Power Generation'. IEEE journal of solid-state circuits, Vol. 33, No.5, May 1998, pp. 687-695.

Blevins, R. D. Formulas for Natural Frequency and Mode Shape. 4th Edition, Robert E. Krieger Publishing Co., Florida. 1987, p.254.

Bendsoe M. P. Optimization of Structural Topology, Shape, and Material, , Springer-Verlag, 1995, pg. 10.

Dosch, J. J., Inman, D. J., Garcia, E. 'A Self-sensing Piezoelectric Actuator for Collocated Control'. Journal of Intelligent Material Systems and Structures, Vol. 3, January 1992, pg.166-185.

Lumsdaine A. and Scott R.A. 'Shape Optimization of Unconstrained Viscoelastic Layers Using Continuum Finite Elements', Journal of Sound and Vibration, Vol. 216(1), , 1998, pg. 29-52.

Rao D. K. 'Frequency and Loss Factors of Sandwich Beams Under Various Boundary Conditions', Journal of Mechanical Engineering Science, Vol. 20, No. 5, 1978, pg. 271-282.

Gao, J. X., Shen, Y. P., and Wang, J. 'Three Dimensional Analysis for Free Vibration of Rectangular Composite Laminates with Piezoelectric Layers'. Journal of Sound and Vibration, Vol. 213, No. 2, 1998, pg. 383-390.

Heyliger P. R. 'Exact Solutions for Simply-Supported Laminated Piezoelectric Plates', Journal of Applied Mechanics, Vol. 64, No. 2, 1997, pg. 299-306

Hofmann, H., Ottman, G. K., and Lesieutre, G. 'A. Optimized Piezoelectric Energy Harvesting Circuit Using Step-Down Converter in Discontinuous Conduction Mode'. 33rd Annual IEEE Power Electronics Specialists Conference, Cairns Convention Centre, Queensland, Australia. June 2002, pg. 1-14.

Ikeda, T. Fundamentals in Piezoelectricity, Oxford Press, Oxford, 1990.

Inman, D. J. Engineering Vibration, 2nd edition, Prentice Hall, 2000.

Inman, D. J., and Cudney, H. H. 'Structural and Machine Design Using Piezoceramic Materials: A Guide for Structural Design Engineers'. Final Report to NASA Langley Research Center, April 30, 2000.

Jaffe, B., Roth, R. S., and Marzullo, S. 'Piezoelectric Properties of Lead Zirconate-Lead Titanate Solid-Solution Ceramics'. Journal of Applied Physics, Vol. 6, No. 25, 1954, pg.809-810.

Journal of Applied Physics, Volume 50, Issue 7, July 1979 , pg. 4904-4912

Kasyap, A., et al. 'Energy Reclamation from a Vibrating Piezoceramic Composite Beam'. Ninth International Congress on Sound and Vibration, ICSV9.

Kendall, C. J. 'Parasitic Power Collection in Shoe Mounted Devices'. Submitted to the Dept. of Physics for fulfillments in Bachelor of Science, Massachusetts Institute of Technology, June 1998.

Kymissis, J., Kendall, C., Paradiso, J., Gershenfeld, N. 'Parasitic Power Harvesting in shoes'. Presented at the second IEEE International conference on wearable computing. Draft 2.0, August 1999.

Lui, G. R., Peng, X. Q., Lam, K. Y.'Vibration Control Simulation of Laminated Composite Plates with Integrated Piezoelectrics'. Journal of Sound and Vibration, Vol. 220, No. 5, 1999, pg. 827-846.

Ottman, G. K., Hofmann, H., Bhatt, A. C., and Lesieutre, G. A.'Adaptive Piezoelectric Energy Harvesting Circuit for Wireless, Remote Power Supply'. IEEE Transactions on Power Electronics, Vol. 17, No. 5, September 2002, pg.1-8.

Rizzoni, G. Principles and Applications of Electrical Engineering, 3rd Ed., McGraw- Hill, 2001.

Sirohi, J., and Chopra, I. 'Fundamental Understanding of Piezoelectric Strain Sensors'. Journal of Intelligent Material Systems and Structures, Vol. 11, April 2000, pg.246- 257.

Smits, J., and Choi, W. 'The Constituent Equations of Piezoelectric Heterogeneous Bi-layers'. IEEE Transactions on Ultrasonics, Ferroelectrics, and Frequency Control, Vol. 38, May 1991, pg.256-270.

Sodano, H., Magliula, E. A., Park, G., and Inman, D. J. 'Electric Power Generation using Piezoelectric Devices'. 13th International Conference on Adaptive Structure and Technologies, 2002.

Umeda, M., Nakamura, K., and Ueha, S. 'Energy Storage Characteristics of a Piezogenerator Using Impact Vibration'. Japan Journal of Applied Physics, Vol. 36, Part 1, No. 5b, May 1997, pg.3146-3151.

Wang, X., Ehlers, C., and Neitzel, M. 'An analytical investigation of static models of piezoelectric patches attached to beams and plates'. Smart Materials and Structures, Vol. 6, 1997, pg.204-213.

Young, D. 'Vibration of Rectangular Plates by the Ritz Method'. Journal of Applied Mechanics, December 1950, pg.448-453.

VITA

Ahmed Mohamed Elalfy was born on 4th of July 1984 in a town called Chingola, Zambia. He attended Nchanga Lower and Upper Trust and School and then transferred to Sacred Heart Convent Secondary School. His secondary school education was completed in accordance with the IGCSE requirements at Lechwe Education Trust in Kitwe, Zambia at which point he was admitted to The University of Tennessee, Knoxville in January 2000. He got his Bachelor of Science Degree in May 2004 from The University of Tennessee, Knoxville. He obtained his Masters of Science Degree in Mechanical Engineering from the University of Tennessee in May 2007.